A Simple Surface Estimation Algorithm for UWB Pulse Radars Based on Trilateration

Michael Mirbach, Wolfgang Menzel
Institute of Microwave Techniques, University of Ulm, PO Box, D-89069 Ulm, Germany
michael.mirbach@uni-ulm.de

***Abstract*—A simple 3D surface estimation algorithm for ultra-wideband (UWB) pulse radars is presented. This algorithm based on trilateration is easy to implement and needs no preprocessing of measurement data. Mathematical derivations of the formulas for both monostatic and bistatic radar imaging setups are derived. The performance of the proposed algorithm is verified in 3D surface measurements, and a good agreement with well-established methods is shown.**

***Index Terms*—3D imaging algorithms, surface estimation, trilateration, ultra-wideband (UWB) pulse radars**

I. Introduction

Ultra-wideband (UWB) pulse radar technology has great potential for imaging and localization applications due to its high range resolution and good non-destructive penetration abilities of dielectric materials. These features make this technology also attractive for medical sensing and imaging applications. One challenge in this field is the localization of objects inside a human body.

In most through-dielectric localization problems like through-the-wall imaging a uniform interface between the two media is assumed. This allows localizing a target without any knowledge about the boundary surface properties [1]. Different localization algorithms like SAR imaging [2] and trilateration can be used to solve this problem. However, with a non-uniform interface the global coherence is lost, and a trilateration method has to be applied [3].

In this paper we investigate if trilateration can be used not only for the localization problem but also for the estimation of the boundary surface. In recent years different highly accurate surface estimation algorithms have been proposed. These imaging algorithms often need complex preprocessing like the Seabed algorithm [4], where wave fronts have to be recognized and estimated [5]. For other approaches, like the Envolope of Spheres algorithm [6], the curvature of the target shape has to be determined first. Recent developments achieved even higher accuracies, however with a significant increase in complexity and computation time [7].

II. Description of the Algorithm

Radar measurements with quasi-omnidirectional antennas only provide information about the target distance, but not about its direction. This makes surface imaging an inverse problem which can only be solved by combining measurement results at different antenna positions. In this case target ranging using trilateration means determining the intersections of spheres of measured target distances. The underlying assumption for utilizing trilateration as a surface estimation method is that two neighboring antennas are "seeing" the same scattering center. As with other imaging algorithms this assumption can lead to inaccuracies of estimated target points.

A. Setup with Monostatic Sensors

The imaging principle shall first be explained using a two-dimensional example. Fig. 1 shows the measurement scenario of a linear array of monostatic radar transceivers arranged along the x-axis scanning the surface of a target varying in z-direction. Each array element is measuring the distance to the closest point on the target. Two exemplary measurement points X_n and X_{n+1} are picked out, and semi circles whose radii correspond to the measured target distances are plotted around the antennas. The wanted target point is the intersection of the two circles.

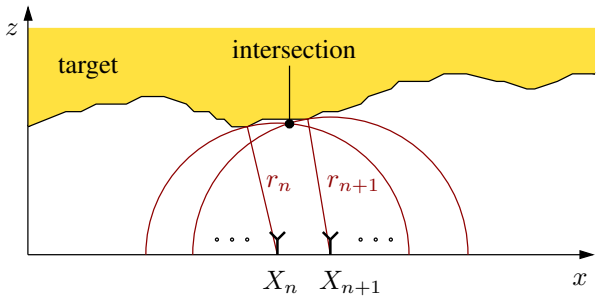

Fig. 1. Cross section of a 2D imaging problem using a linear array of monostatic radar transceivers along the x-axis. Two exemplary measurements at the positions X_n and X_{n+1} illustrate target point estimation by trilateration.

Three-dimensional imaging demands for a third antenna position which has to be located in a different dimension. This setup is shown as a top view in Fig. 2. At each of the three points a target distance r_i is measured which leads to a set of spheres with radii r_i around the respective antenna position A_i, as defined by the equation system

$$r_1^2 = x^2 + y^2 + z^2 \quad (1)$$
$$r_2^2 = (x-d)^2 + y^2 + z^2 \quad (2)$$
$$r_3^2 = x^2 + (y-j)^2 + z^2, \quad (3)$$

where d and j are the distances between two antennas in x- and y-direction, respectively. For simplicity, the first antenna position A_1 shall be at the center of the coordinate system.

The above equation system is valid for a planar antenna array. In case of a curved antenna array an offset z-value has to be inserted.

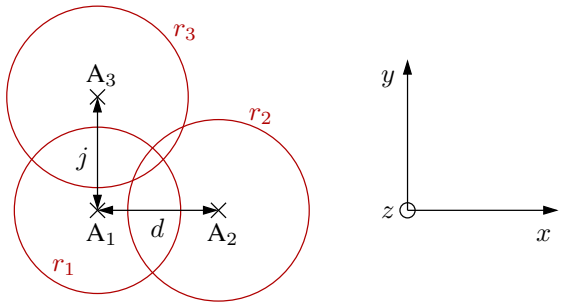

Fig. 2. Top view of three measuring points of an antenna array in the x-y-plane. At each antenna position $A_{1\text{-}3}$ a target distance $r_{1\text{-}3}$ is measured.

The initial assumption that all three antennas are "seeing" the same target has to be assured by comparing the measured target distances $r_{1\text{-}3}$. If the difference between these distances is small enough the assumption can be considered valid. For the above equations this precondition can be formulated as follows:

$$|r_1 - r_2| \leq T_{s,x} \quad \text{and} \quad |r_1 - r_3| \leq T_{s,y} \tag{4}$$

A threshold T_s in the range of about half the antenna distance has shown good results.

If the conditions in (4) are fulfilled, the target surface point of interest can be calculated by intersecting the three spheres. The coordinates (x, y, z) of the intersection are

$$x = \frac{r_1^2 - r_2^2 + d^2}{2d} \tag{5}$$

$$y = \frac{r_1^2 - r_3^2 + j^2}{2j} \tag{6}$$

$$z = \pm\sqrt{r_1^2 - x^2 - y^2}. \tag{7}$$

These coordinates are offsets refering to the position of the first antenna A_1. The sign in (7) depends on the arrangement of the radar transceivers. In the following we assume that the antennas are oriented to positive z-values.

B. Setup with Bistatic Sensors

When performing bistatic radar measurements the targets have to be located on the shells of ellipsoids instead of spheres. Fig. 3 illustrates the cross section of the ellipsoid obtained by a bistatic radar measurement with two antennas at the positions X_t and X_r. With the measured time-of-flight of the transmitted pulse, corresponding to r_1+r_2, and the spacing e between transmitter and receiver, the equatorial radii defining the ellipsoid can be calculated as follows:

$$a = \frac{r_1 + r_2}{2} \tag{8}$$

$$b = \sqrt{a^2 - \left(\frac{e}{2}\right)^2} \tag{9}$$

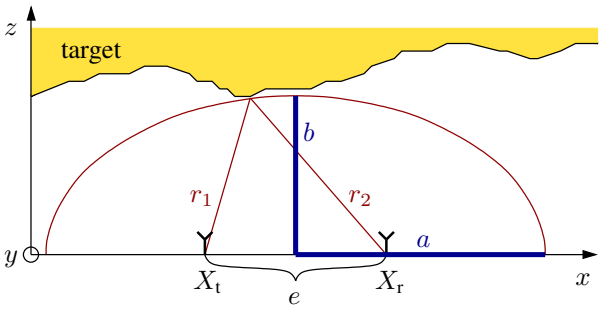

Fig. 3. Cross section of an ellipsoid of possible target locations for one bistatic radar measurement with the antenna spacing e. The parameters a and b are the equatorial radii of the ellipsoid.

The ellipsoid is rotation-symmetric with respect to the x-axis, so the parameter b is also valid in y-direction.

In analogy to Fig. 2 and eq. (1)–(3) the system of equations of the three ellipsoids needed for trilatation is

$$\frac{x^2}{a_1^2} + \frac{y^2}{b_1^2} + \frac{z^2}{b_1^2} = 1 \tag{10}$$

$$\frac{(x-d)^2}{a_2^2} + \frac{y^2}{b_2^2} + \frac{z^2}{b_2^2} = 1 \tag{11}$$

$$\frac{x^2}{a_3^2} + \frac{(y-j)^2}{b_3^2} + \frac{z^2}{b_3^2} = 1. \tag{12}$$

In order to solve the system of equations we subtract (10) from (11) and get

$$\underbrace{\left(\frac{b_1^2}{a_1^2} - \frac{b_2^2}{a_2^2}\right)}_{A} x^2 + \underbrace{\frac{2db_2^2}{a_2^2}}_{B} x \underbrace{- \frac{d^2 b_2^2}{a_2^2} - b_1^2 + b_2^2}_{C} = 0. \tag{13}$$

The wanted target coordinates (x, y, z) are now calculated to

$$x = \begin{cases} -\frac{C}{B}, & \text{if } A = 0, \\ \frac{-B+\sqrt{B^2-4AC}}{2A}, & \text{otherwise.} \end{cases} \tag{14}$$

$$y = -\frac{1}{2j}\left(\left(\frac{b_1^2}{a_1^2} - \frac{b_3^2}{a_3^2}\right)x^2 - j^2 - b_1^2 + b_3^2\right) \tag{15}$$

$$z = \pm\sqrt{-\frac{b_1^2}{a_1^2}x^2 - y^2 + b_1^2}. \tag{16}$$

Obviously the additional parameters a and b, connected to the bistatic antenna spacing e, lead to more complex formulas compared to those of a monostatic radar setup.

C. Formulation of the Algorithm

The necessary steps of the proposed trilateration algorithm can be summarized as follows, using the example of a monostatic radar setup:

1) Pick three neighboring measurement points in two different dimensions (here: along the x- and y-axis).
2) Extract the target distance from the recorded radar measurement data at each antenna position. Multiple target responses per measurement are possible.

3) Check if the differences between the measured distances satisfy the trilateration condition in eq. (4).
4) If the previous condition is fulfilled, calculate the target coordinates using eq. (5)-(7).
5) Repeat the two previous steps if higher order reflections exist, or otherwise start over with the next three measurement positions.

III. Measurement Results

The radar measurements for the evaluation of the proposed algorithm have been performed using a custom built bistatic radar sensor [8] for the FCC UWB frequency mask. It transmits a 1st derivative of a Gaussian pulse and uses a correlation receiver to determine the target distance. Both the transmitter and the receiver are equipped with a planar Vivaldi antenna. Fig. 4 shows a typical correlation signal obtained with a plane metal target at a distance of about 29 cm. The amplitudes in the range from 0 cm to 10 cm are due to coupling between the transmitting and the receiving antenna.

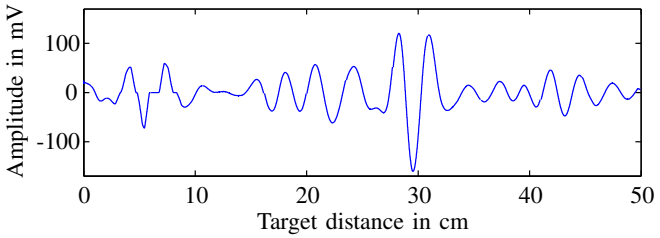

Fig. 4. Correlation output of the radar sensor. The antennas are placed in front of a plane metal plate at a distance of 29 cm.

In the measurements presented here, an array of radar transceivers is simulated by performing linear scans with only one transceiver element. For every measurement position of the scan the correlation is evaluated, and one or more target distances are extraced depending on the correlation strength.

A. Measurements in 2D

In a 2D setup the equivalent of the above mentioned trilateration procedure is the calculation of intersection points of circles. Fig. 5 shows 108 semi circles obtained from monostatic radar measurments with the transceiver moving along the x-axis between the coordinates -60 cm and 0 cm. The step width between each measurement was 0.5 cm resulting in a total of 121 measuring points.

The calculated intersections of these semi circles are displayed in Fig. 6. These estimated points show a good agreement with both, the ideal target shape and the results of the Seabed algorithm which are illustrated in Fig. 7. The points obtained with Seabed show a much smoother alignment because this algorithm evaluates wave fronts which can be interpolated once they are recognized leading to more uniform estimated shapes. This advantage, however, is only given for the clear wave fronts of simple geometric shapes and becomes less significant when trying to estimate more complex shapes.

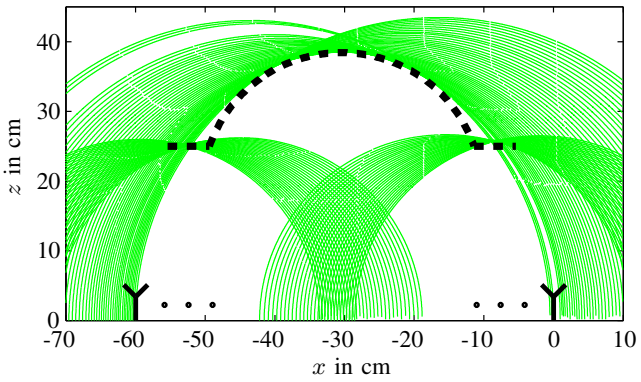

Fig. 5. Set of semi circles of measured target distances. The dashed line describes the shape of the target object.

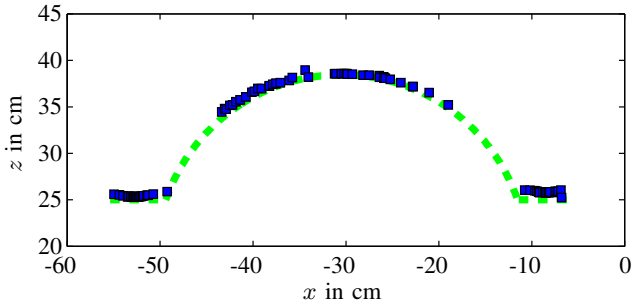

Fig. 6. Estimated shape points obtained by the calculation of the intersections of the above set of circles.

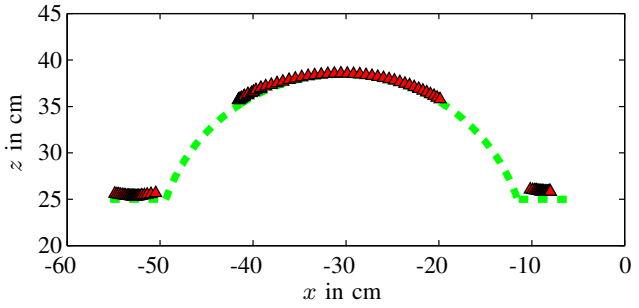

Fig. 7. Estimated shape points of the same measurement using the Seabed algorithm.

B. Measurements in 3D

3D surface measurements have been performed using linear radar scans in two dimensions. As a target object a plastic dummy of a male torso of about 60 cm height has been chosen. In order to increase the target's reflectivity the surface of the dummy has been treated with conductive copper laquer.

Fig. 8 and 9 show the estimated surface points using the three aforementioned algorithms Seabed, Envelope of Spheres, and trilateration. The step width between each measurement position was 1 cm with a total number of 2856 measurements. The trilateration algorithm generated 1084 surface points, the Seabed and Envelope of Spheres algorithms 852 and 2687 points, respectively. The reason for the high number of

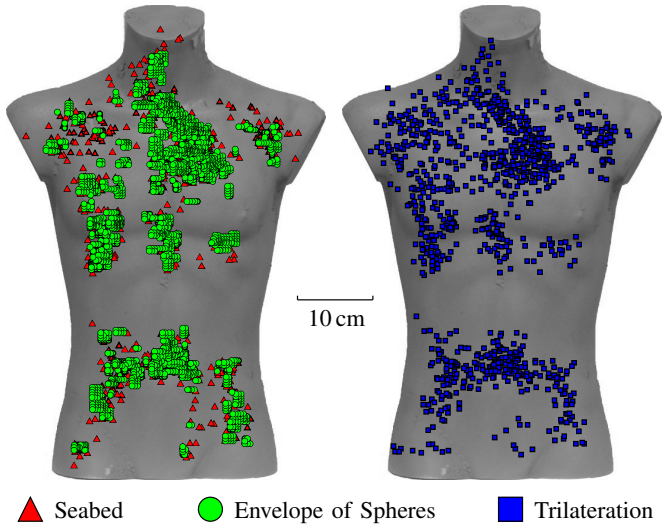

Fig. 8. Estimated surface points using the Seabed, the Envolope of Spheres, and the proposed trilateration algorithms for the measurement of a human torso dummy with a planar antenna array.

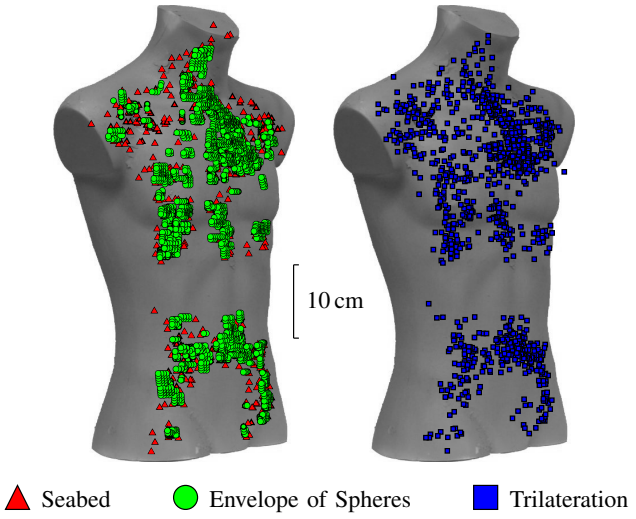

Fig. 9. View of the above estimated target points rotated by 45°.

estimated points using the latter algorithm lies in the nature of the applied method and does not neccessarily imply that more information about the target surface has been gained. This can also be seen in Fig. 8 and 9, where the area covered by estimated surface points is about the same for all three algorithms. What can be observed as well is that the results of the proposed trilateration method agree very well with the data obtained using the established imaging algorithms.

C. Examination of Surface Estimation Errors

The accuracy of the three algorithms has been compared measuring the surface of a metal sphere with a known diameter of 35 cm. For the comparison of bistatic measurements the Envelope of Spheres algorithm has been modified to an algorithm using the envelope of ellipsoids. The error distance between estimated points and the ideal surface of the target sphere has been calculated and plotted in Fig. 10–13 for monostatic and bistatic radar measurements and for different densities of measurement points. The graphs show the percentage of estimated points having a certain deviation in cm from the ideal surface. In order to compare the results of the different algorithms at exactly the same coordinates, the estimated points have been interpolated on an identical coordinate grid covering the whole area of the estimated surface.

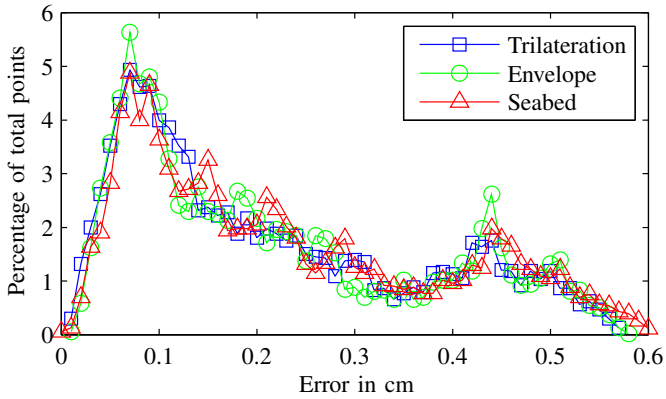

Fig. 10. Percentaged distribution of the difference between estimated and ideal surface points for different imaging algorithms in a monostatic radar setup with the distance d=1.5 cm between measuring points.

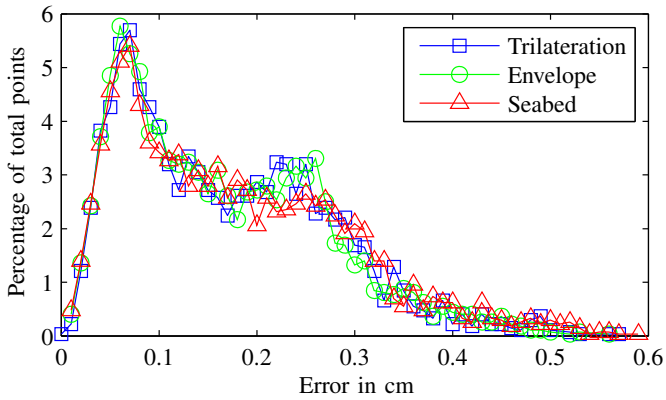

Fig. 11. Percentaged distribution of the difference between estimated and ideal surface points for different imaging algorithms in a bistatic radar setup with the distance d=1.5 cm between measuring points.

TABLE I
ROOT MEAN SQUARE ERROR (RMSE) OF THE MEASUREMENTS PRESENTED IN FIG. 10–13.

Measurement series	Trilateration	Envelope	Seabed
Monostatic, d=1.5 cm	0.259 cm	0.265 cm	0.272 cm
Bistatic, d=1.5 cm	0.199 cm	0.196 cm	0.209 cm
Monostatic, d=6 cm	0.127 cm	0.169 cm	0.338 cm
Bistatic, d=6 cm	0.166 cm	0.171 cm	0.253 cm

While in the first two measurements in Fig. 10 and 11 a relatively small step width of d=1.5 cm between two measuring postions has been used, the measurement results in Fig. 12 and 13 show the errors obtained with a quadrupled step width of

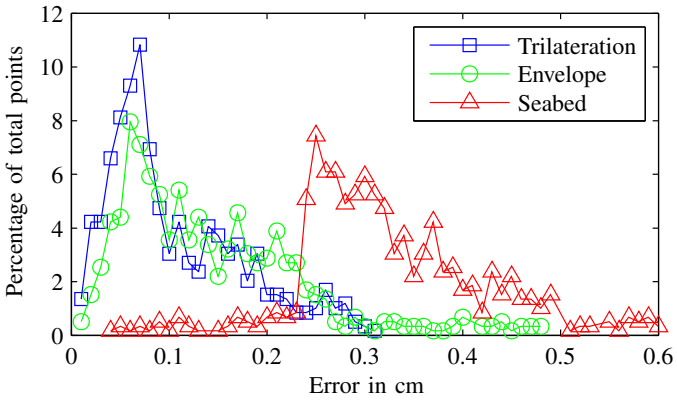

Fig. 12. Percentaged distribution of the difference between estimated and ideal surface points for different imaging algorithms in a monostatic radar setup with an increased distance d=6 cm between measuring points.

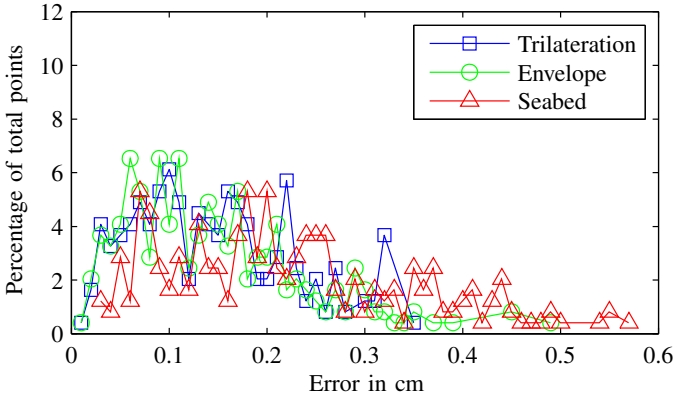

Fig. 13. Percentaged distribution of the difference between estimated and ideal surface points for different imaging algorithms in a bistatic radar setup with an increased distance d=6 cm between measuring points.

6 cm. In the bistatic setups the spacing e between transmitting and receiving antenna has been 30 cm. Table I displays the calculated root mean square errors (RMSE) of each series of measurement.

In Fig. 10 and 11 it can be seen that with a high density of measurement points there is no significant difference of estimation errors between the algorithms. The deviations from the ideal surface points are in a low millimeter range. However, with an increased distance between measurement points the performance of Seabed is degrading significantly, while the errors obtained with trilateration and the Envelope of Spheres algorithm remain in the same range.

IV. Conclusion

A 3D surface estimation algorithm based on trilateration for ultra-wideband pulse radars has been presented and derived mathematically. Unlike other imaging algorithms, this method needs no preprocessing of measurement data which simplyfies its implementation. Formulas for both, monostatic and bistatic radar imaging have been given. In 3D surface measurements the performance of the proposed algorithm has been verified and comparisons with established algorithms have shown a good agreement between the respective results. The estimation errors of all compared methods have been analyzed using different densities of measurement points, where the proposed algorithm has always achieved one of the lowest errors. The proposed algorithm has therefore proved to be a qualified alternative for fast and easy surface imaging.

V. Acknowledgment

This work has been funded by the German Research Foundation (DFG) under the program UKoLoS.

References

[1] F. Ahmad and M. G. Amin, "Noncoherent approach to through-the-wall radar localization," *IEEE Transactions on Aerospace and Electronic Systems*, vol. 42, no. 4, pp. 1405–1419, 2006.

[2] G. L. Charvat, L. C. Kempel, E. J. Rothwell, C. M. Coleman, and E. L. Mokole, "A through-dielectric radar imaging system," *Antennas and Propagation, IEEE Transactions on*, vol. 58, no. 8, pp. 2594–2603, 2010.

[3] N. Maaref, P. Millot, C. Pichot, and O. Picon, "Through-the-wall radar using multiple uwb antennas," in *IET Conference Publications*, 2007.

[4] T. Sakamoto, "A fast algorithm for 3-dimensional imaging with uwb pulse radar systems," *IEICE Transactions on Communications*, vol. E90-B, no. 3, pp. 636–644, 2007.

[5] S. Hantscher, B. Etzlinger, A. Reisenzahn, and C. G. Diskus, "A wave front extraction algorithm for high-resolution pulse based radar systems," in *2007 IEEE International Conference on Ultra-Wideband, ICUWB*, 2007, pp. 590–595.

[6] S. Kidera, T. Sakamoto, and T. Sato, "High-resolution 3-d imaging algorithm with an envelope of modified spheres for uwb through-the-wall radars," *Antennas and Propagation, IEEE Transactions on*, vol. 57, no. 11, pp. 3520–3529, 2009.

[7] ——, "Accurate uwb radar three-dimensional imaging algorithm for a complex boundary without range point connections," *Geoscience and Remote Sensing, IEEE Transactions on*, vol. 48, no. 4, pp. 1993–2004, 2010.

[8] M. Leib, E. Schmitt, A. Gronau, J. Dederer, B. Schleicher, H. Schumacher, and W. Menzel, "A compact ultra-wideband radar for medical applications," *Frequenz*, vol. 63, no. 1-2, pp. 2–8, 2009.